iScience

CellPress
OPEN ACCESS

Article

hESC- and hiPSC-derived Schwann cells are molecularly comparable and functionally equivalent

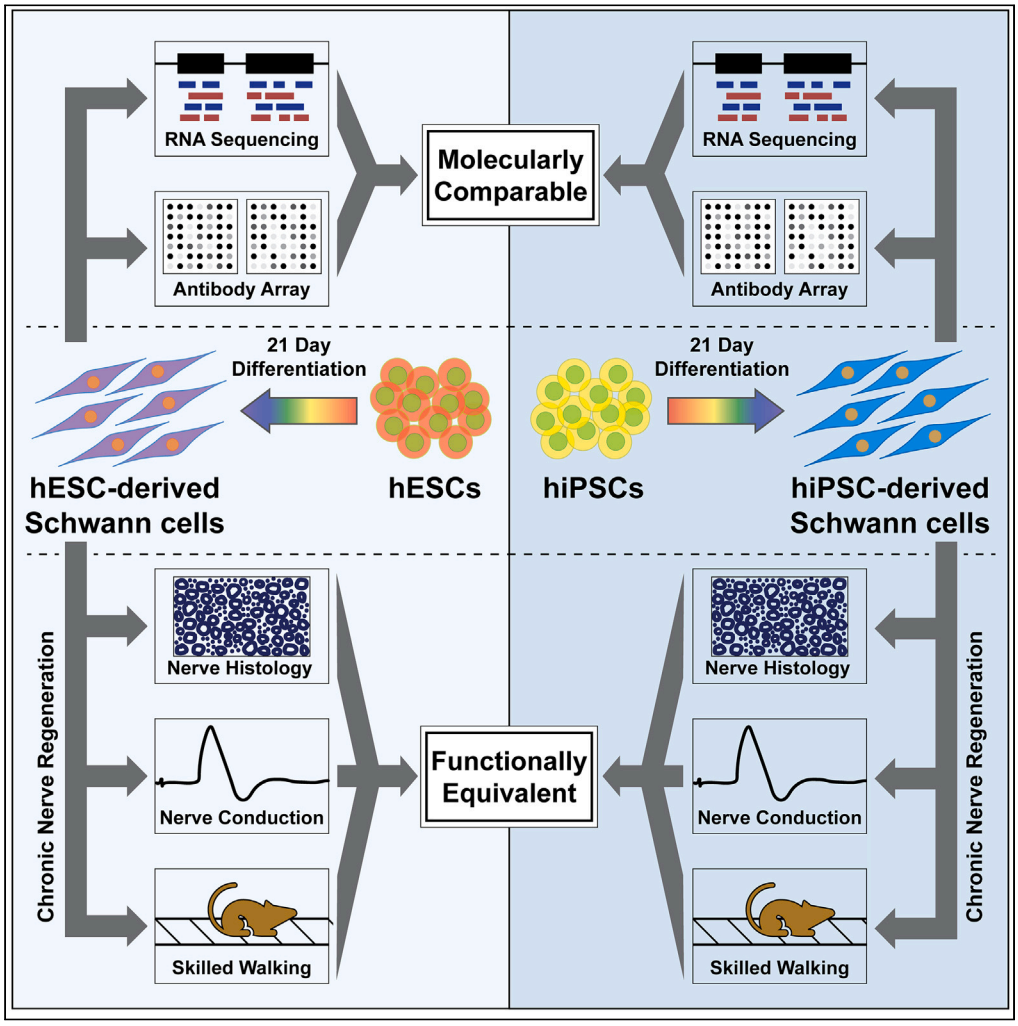

Kathryn R. Moss, Ruifa Mi, Riki Kawaguchi, ..., Bipasha Mukherjee-Clavin, Gabsang Lee, Ahmet Höke

ahoke@jhmi.edu

Highlights

RNA sequencing and antibody array data from hESC- and hiPSC-derived Schwann cells

HESC- and hiPSC-derived Schwann cells exhibit minimal transcriptome differences

No proteome differences by antibody array in hESC- and hiPSC-derived Schwann cells

hESC- and hiPSC-derived Schwann cells equally promote regeneration *in vivo*

Moss et al., iScience 27, 109855
June 21, 2024
https://doi.org/10.1016/j.isci.2024.109855

iScience

CellPress
OPEN ACCESS

Article

hESC- and hiPSC-derived Schwann cells are molecularly comparable and functionally equivalent

Kathryn R. Moss,[1] Ruifa Mi,[1] Riki Kawaguchi,[2] Jeffrey T. Ehmsen,[1] Qiang Shi,[1] Paula I. Vargas,[1] Bipasha Mukherjee-Clavin,[1] Gabsang Lee,[1,3,4] and Ahmet Höke[1,3,5,*]

SUMMARY

Establishing robust models of human myelinating Schwann cells is critical for studying peripheral nerve injury and disease. Stem cell differentiation has emerged as a key human cell model and disease motivating development of Schwann cell differentiation protocols. Human embryonic stem cells (hESCs) are considered the ideal pluripotent cell but ethical concerns regarding their use have propelled the popularity of human induced pluripotent stem cells (hiPSCs). Given that the equivalence of hESCs and hiPSCs remains controversial, we sought to compare the molecular and functional equivalence of hESC- and hiPSC-derived Schwann cells generated with our previously reported protocol. We identified only modest transcriptome differences by RNA sequencing and insignificant proteome differences by antibody array. Additionally, both cell types comparably improved nerve regeneration and function in a chronic denervation and regeneration animal model. Our findings demonstrate that Schwann cells derived from hESCs and hiPSCs with our protocol are molecularly comparable and functionally equivalent.

INTRODUCTION

Myelinating Schwann cell models are required to understand demyelinating diseases and axon regeneration in the peripheral nervous system. Developing human models is ideal given that translating findings from rodents to humans has proven difficult (i.e., ascorbic acid clinical trials for CMT1A).[1] Schwann cells can be harvested from human nerve biopsies, but this procedure is invasive and yields a finite quantity of cells. Therefore, a more practical strategy is to generate human Schwann cells from pluripotent cells. Although human embryonic stem cells (hESCs) are considered the gold standard with respect to pluripotency, ethical concerns over their use make human induced pluripotent stem cells (hiPSCs) a more attractive approach.[2,3] However, the equivalence of hESCs and hiPSCs is a much-debated topic.[4] Therefore, it is essential to determine if hESCs and hiPSCs differentiated with a particular protocol demonstrate molecular and functional equivalence.

We have developed a differentiation protocol that generates sufficient quantities of Schwann cells that can subsequently be purified by fluorescence-activated cell sorting (FACS) for α4-integrin CD49d (CD49d) expression.[5] Here, we generated hESC- and hiPSC-derived Schwann cells using our established protocol and performed transcriptomic, proteomic, and functional comparisons of these cells. Three established hESC lines and three iPSC lines previously generated from healthy control dermal fibroblasts were used. The hESC and hiPSC lines were efficiently differentiated into Schwann cells as demonstrated by expression of Schwann cell markers by immunocytochemistry and RNA sequencing. Differential expression analysis of the RNA sequencing dataset revealed only modest transcriptome differences and antibody array demonstrated insignificant proteome differences. hESC- and hiPSC-derived Schwann cell function was evaluated in a chronic denervation and regeneration animal model followed by behavioral, electrophysiological, and histological assessment. Transplantation of hESC- and hiPSC-derived Schwann cells equally improved nerve regeneration and function as compared to transplantation of heat killed hESC- and hiPSC-derived Schwann cells demonstrating functional equivalence of these cells.

RESULTS

hESC and iPSC Schwann cell differentiation

Our previously established 21-day differentiation protocol was used to generate hESC- and hiPSC-derived Schwann cells (Figure 1A).[5] Three common hESC lines were used (H1 [male], H7 [female] and H9 [female]) and three iPSC lines previously generated from healthy control dermal

[1]Department of Neurology, Neuromuscular Division, Johns Hopkins University School of Medicine, Baltimore, MD 21205, USA
[2]Semel Institute for Neuroscience and Human Behavior, University of California, Los Angeles, Los Angeles David Geffen School of Medicine, Los Angeles, CA 90095, USA
[3]Department of Neuroscience, Johns Hopkins University School of Medicine, Baltimore, MD 21205, USA
[4]Institute for Cell Engineering, Johns Hopkins University School of Medicine, Baltimore, MD 21205, USA
[5]Lead contact
*Correspondence: ahoke@jhmi.edu
https://doi.org/10.1016/j.isci.2024.109855

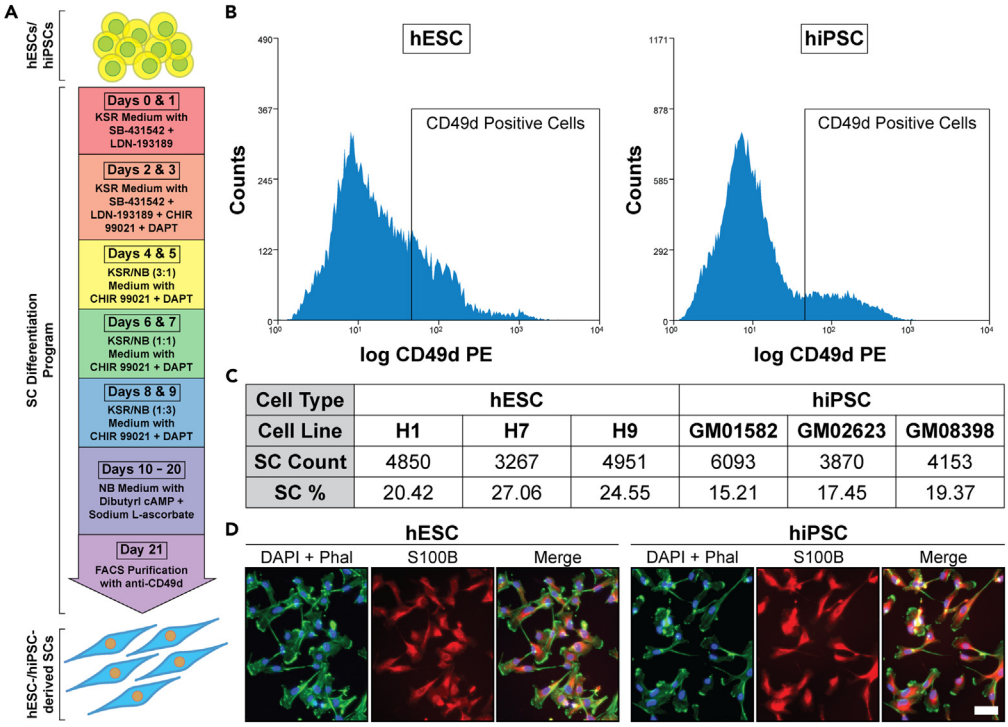

Cell Type	hESC			hiPSC		
Cell Line	H1	H7	H9	GM01582	GM02623	GM08398
SC Count	4850	3267	4951	6093	3870	4153
SC %	20.42	27.06	24.55	15.21	17.45	19.37

Figure 1. hESC and hiPSC cells are efficiently differentiated into Schwann cells

(A) Diagram of the 21-day Schwann cell differentiation protocol.

(B) Representative cells count graphs of CD49d FACS sorted hESC- and hiPSC-derived Schwann cells.

(C) Representative Schwann cell differentiation efficiencies for each hESC and hiPSC line (n = 1 each).

(D) Representative images of passage two CD49d-positive hESC- and hiPSC-derived Schwann cells processed for immunocytochemistry with an anti-S100B antibody (red), Phalloidin to label F-actin (green) and DAPI (blue). Scale bar, 50μm.

fibroblasts were used (GM01582 [11-year-old female donor], GM02623 [61-year-old female donor] and GM08398 [8-year-old male donor]). CD49d-positive Schwann cells were purified by FACS.[5] Representative CD49d-positive cell counts demonstrate a relatively high differentiation efficiency for both hESCs and hiPSCs (15–27%, Figures 1B and 1C). However, comparing the differentiation efficiency between hESCs and hiPSCs is difficult to interpret due to multiple variables introduced by FACS sorting. Purified hESC- and hiPSC-derived Schwann cells were cultured and immunocytochemistry was performed at passage two to evaluate cell morphology and expression of the Schwann cell marker S100B (Figure 1D). Both hESC- and hiPSC-derived Schwann cells exhibit bi/tripolar morphology akin to cultured primary Schwann cells and highly express S100B.

Modest transcriptome differences between hESC- and iPSC-derived Schwann cells

RNA was isolated from passage two hESC- and hiPSC-derived Schwann cells and transcriptome analysis was performed by RNA sequencing. One independent replicate for each stem cell line was included with three total hESC lines (n = 3) compared to three total hiPSC lines (n = 3). mRNA levels for each gene were averaged and compared between hESC- and hiPSC-derived Schwann cells. To confirm proper differentiation of the hESCs and hiPSCs into Schwann cells, Fragments Per Kilobase Million (FPKM) values of Schwann cell markers were analyzed. FPKM values for the integral Schwann cell/myelin genes *Dystonin* (*DST*, p = 0.9193), *Myelin Basic Protein* (*MBP*, p = 0.8058), *Peripheral Myelin Protein 22* (*PMP22*, p = 0.8265), *Erb-B2 Receptor Tyrosine Kinase 2* (*ERBB2*, p-0.9112) and *Nerve Growth Factor Receptor* (*NGFR*, p = 0.7581) were averaged and compared between hESC- and hiPSC-derived Schwann cells (Figure 2A). Comparing these average FPKM values to the ubiquitous genes *Histone 1, H1b* (*HIST1H1B*, hESC FPKM: Mean = 259.00, SD = 75.19; hiPSC FPKM: Mean = 245.20, SD = 151.30) and *ATP Synthase F1 Subunit Alpha* (*ATP5A1*, hESC FPKM: Mean = 32.30, SD = 3.65; hiPSC FPKM: Mean = 30.63, SD = 4.28) demonstrates relatively high expression of the Schwann cell/myelin genes.

Differential expression analysis of our dataset identified 142 genes (FDR-adjusted $p < 0.05$); 20 genes demonstrated significantly higher mRNA levels in hESC-derived Schwann cells and 122 genes demonstrated significantly higher mRNA levels in hiPSC-derived Schwann cells (Figure 2B; Table S2). 16,590 genes were comparably expressed between hESC- and hiPSC-derived Schwann cells, including 46 integral Schwann cell genes (Figure S1A; Table S1). Ingenuity Pathway Analysis was performed on the 142 significant genes to identify significant canonical pathways (Figure 2C; Table S3). Both the significant genes and significant canonical pathways were further investigated for links to

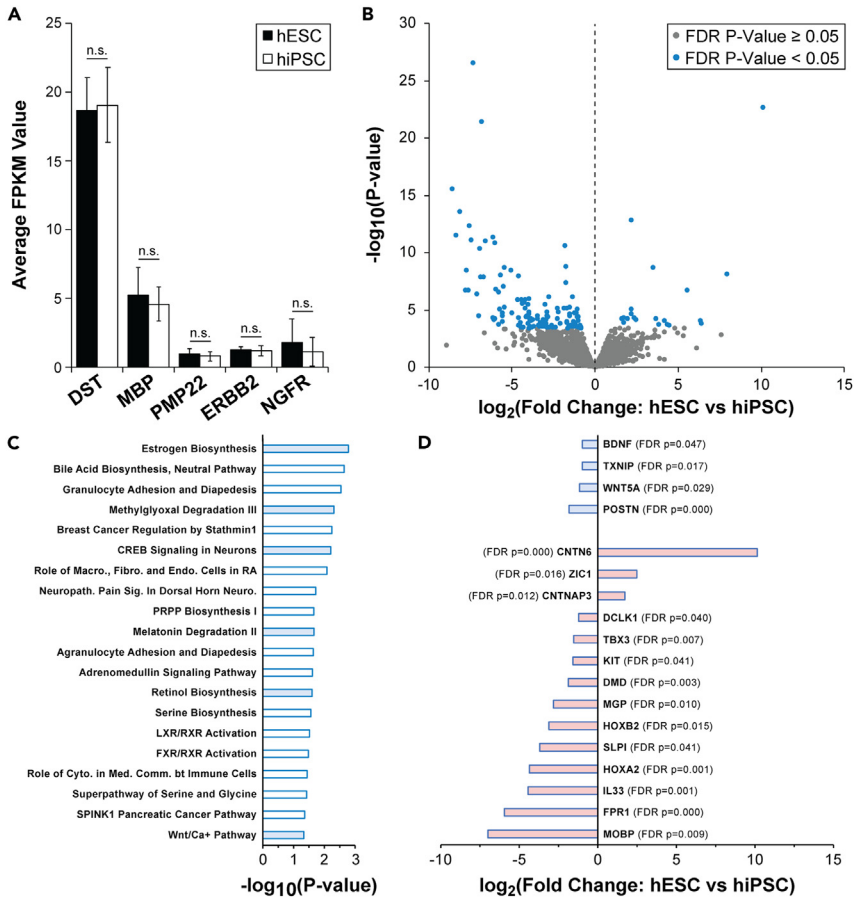

Figure 2. Minimal transcriptome differences between hESC- and hiPSC-derived Schwann cells

RNA was isolated from passage two hESC- and hiPSC-derived Schwann cells and RNA sequencing was performed. mRNA levels for each gene were averaged and compared between hESC- and hiPSC-derived Schwann cells (n = 1 per stem cell line, n = 3 per stem cell type).

(A) Average FPKM values of integral Schwann cell/myelin genes. Data are represented as mean ± SEM. Equal variance was confirmed by F-test analysis. Unpaired t-test, n.s. = not significant ($p > 0.05$).

(B) Differential expression analysis data displayed by volcano plot. Blue data points are statistically significant (142 genes, FDR-adjusted $p < 0.05$).

(C) Statistically significant canonical pathways identified by Ingenuity Pathway Analysis for the 142 significant genes. Light blue bars have demonstrated links to Schwann cell/myelin function whereas white bars do not.

(D) Significant differentially expressed genes with concrete (light blue bars) and potential (light pink bars) links to Schwann cell/myelin function. FDR-adjusted p-value are shown in parentheses.

Schwann cell/myelin function. A link was established for the following canonical pathways: Estrogen Biosynthesis,[6] Methylglyoxal Degradation III,[7] CREB Signaling in Neurons,[8] Melatonin Degradation II,[9,10] Retinol Biosynthesis[11] and Wnt/Ca+ Pathway[12] (Figure 2C). However, *Wnt Family Member 5A* (*WNT5A*, higher expression in iPSC-derived Schwann cells, FDR-adjusted $p = 0.0289$) is the only canonical pathway-implicated gene that is directly involved in Schwann cell function, specifically proliferation[12] (Figure 2D; Tables S2 and S3). *Interleukin 33* (*IL33*, higher expression in iPSC-derived Schwann cells, FDR-adjusted $p = 0.0007$) and potentially *Formyl Peptide Receptor 1* (*FPR1*, higher expression in iPSC-derived Schwann cells, FDR-adjusted $p = 0.0001$) are canonical pathway-implicated genes that are involved in oligodendrocyte function suggesting they may also play a role in Schwann cells[13,14] (Figure 2D; Tables S2 and S3). Of the remaining significant genes, only three have been demonstrated to have a clear connection to Schwann cells: *Periostin* (*POSTN*, higher expression in iPSC-derived Schwann cells, FDR-adjusted $p = 3.69\text{x}10^{-8}$), *thioredoxin interacting protein* (*TXNIP*, higher expression in iPSC-derived Schwann cells, FDR-adjusted $p = 0.0170$) and *brain-derived neurotrophic factor* (*BDNF*, higher expression in iPSC-derived Schwann cells, FDR-adjusted $p = 0.0465$) (Figure 2D; Table S2). POSTN and TXNIP are involved in Schwann cell migration[15,16] whereas BDNF plays a role in Schwann cell proliferation, migration and myelination.[17–19] Twelve additional genes are potentially involved in Schwann cell/myelin function and/or play a role in oligodendrocytes (Figure 2D; Table S2).

Given that many more genes demonstrate significantly increased mRNA levels in hiPSC-derived Schwann cells (122 increased in hiPSC, 20 increased in hESC), we also performed GO enrichment analysis on both sets of genes to help interpret this result.[20–22] There was no significant

enrichment for biological processes or molecular functions with the genes demonstrating increased mRNA levels in hESC-derived Schwann cells. However, there was significant enrichment for both biological processes and molecular functions with the genes demonstrating increased mRNA levels in hiPSC-derived Schwann cells. The significantly enriched biological processes are all generally related to development and the only two involving the nervous system are cranial nerve morphogenesis (GO:0021602, FDR-adjusted $p = 0.0356$) and rhombomere development (GO:0021546, FDR-adjusted $p = 0.0421$) (Table S4). The significantly enriched molecular functions relate to DNA binding and transcription (Table S5). Taken together, our results indicate that there are minimal transcriptome differences between hESC- and hiPSC-derived Schwann cells and most of the significantly differentially expressed genes do not to have a bona fide or potential link to Schwann cell/myelin function.

We also evaluated the robustness of our differentiation protocol and confirmed the Schwann cell identity of our cells by generating Schwann cells from one hESC line (H9) and one hiPSC line (GM02623) and performing a second set of RNA sequencing with passage two cells using three independent replicates from each. FPKM values for Schwann cell markers were then compared between hESC- and hiPSC-derived Schwann cells and between RNA sequencing sets one and two. FPKM values from published datasets with rat Schwann cells were also included as a reference (data accessible at NCBI GEO database,[23] accession numbers GSE211336 [24] and GSE177037 [25]). Comparing the FPKM values for *DST*, *MBP*, *PMP22*, *ERBB2*, *NGFR*, *AHNAK Nucleoprotein* (*AHNAK*), *S100 Calcium Binding Protein A6* (*S100A6*), and *S100 Calcium Binding Protein A10* (*S100A10*) from RNA sequencing sets one and two demonstrates that our hESC- and hiPSC-derived Schwann cells express Schwann cell markers although generally at lower levels than primary rodent Schwann cells suggesting our cells are immature Schwann cells (Figure S1B; Table S6). And although there is some variability, there is no statistically significant difference between hESC- and hiPSC-derived Schwann cells or between sets one and two (Figure S1B). These results demonstrate the reproducibility of our differentiation protocol to generate Schwann cells.

Insignificant proteome differences between hESC- and iPSC-derived Schwann cells

Cell lysates were collected from passage three hESC- and hiPSC-derived Schwann cells and proteome analysis was performed by antibody array. One independent replicate for each stem cell line was included with three total hESC lines ($n = 3$) compared to three total hiPSC lines ($n = 3$). Lysates were biotinylated and incubated with two membranes containing a total of 1000 antibodies recognizing human proteins. Relative protein levels were determined by immunoblotting for HRP-conjugated Streptavidin. Signal intensity for each protein was averaged and compared between hESC- and hiPSC-derived Schwann cells. This analysis identified zero proteins that were significantly differentially expressed ($p < 0.05$, Figures 3A and 3B; Table S7). Interestingly, pro-BDNF ($p = 0.6219$), BDNF ($p = 0.7774$), IL33 ($p = 0.6219$), five canonical pathway-implicated genes (none of which are directly linked to Schwann cell function: CCL26, CCL28, MMP1, SAA1, IL24; $p = 0.7774$, 0.9260, 0.7774, 0.6917, 0.5275, respectively) and SLPI (one of the twelve genes potentially linked to Schwann cell function, $p = 0.4471$) protein levels were included in the antibody array. These results suggest that some of the significantly differentially expressed genes identified by RNA sequencing do not exhibit altered protein expression. Although several proteins demonstrated a large difference between hESC- and hiPSC-derived Schwann cells, none were significant due to high variability likely attributed to human genetic complexity (Figure 3B; Table S7). The proteins that were most divergently expressed and nearest to statistical significance are graphed in Figures 3C and 3D. Given the large variability, the 18 most divergent expressed proteins and 4 proteins nearest to statistical significance were assessed for equal variance by F-test analysis. Btk, FGFR1 and BNP are the only proteins in this group with unequal variance (Figures 3C and 3D). The antibody array data for all proteins were also analyzed by unpaired t-test with Welch correction to account for potential unequal variance but no significant differentially expressed proteins were identified (Table S8). And only a portion of most divergently expressed and nearest to statistical significance proteins have been linked to Schwann cell/myelin function: Fibronectin ($p = 0.4089$), Fibrinogen ($p = 0.3715$) and Integrin alpha V ($p = 0.5132$) for extracellular matrix,[26–28] FGFR1 ($p = 0.4121$) for differentiation and migration,[29,30] BNP ($p = 0.3772$) for proliferation[31] and Progranulin ($p = 0.1625$) and MIF ($p = 0.1303$) for nerve regeneration[32,33] (Figures 3C and 3D).

Functional equivalence of hESC- and iPSC-derived Schwann cells

Given that hESC- and hiPSC-derived Schwann cells are molecularly comparable, the functional equivalence was evaluated. A chronic denervation and regeneration mouse model was used to determine the ability of hESC- and hiPSC-derived Schwann cells to enhance peripheral nerve regeneration *in vivo*.[34] Alive and heat killed hESC- and hiPSC-derived Schwann cells were transplanted and regeneration of the transected peroneal nerve into the denervated tibial nerve was evaluated histologically, electrophysiologically and behaviorally. The average number of myelinated axons regenerated 5-7mm distal to the peroneal-tibial nerve repair site was equivalent between alive hESC- and hiPSC-derived Schwann cells ($p = 0.9939$, Figures 4A and 4B). Regenerated myelinated axons were also equivalent between heat killed hESC- and hiPSC-derived Schwann cells ($p = 0.8341$) but were significantly increased with alive hESC- and hiPSC-derived Schwann cell transplantation as compared to heat killed ($p = 0.0005$, Figures 4A and 4B). Sciatic nerve compound muscle action potentials (CMAPs) recorded from the distal foot muscles exhibited comparable amplitudes and latencies with alive hESC- and hiPSC-derived Schwann cells (amp. $p = 0.8458$, lat. $p = 0.1988$, Figures 4C–4E). Again, CMAP amplitudes and latencies were comparable between heat killed hESC- and hiPSC-derived Schwann cells (amp. $p = 0.9606$, lat. $p = 0.7916$) but amplitudes were significantly increased ($p = 0.0033$) and latencies were significantly reduced ($p = 0.0092$) with alive hESC- and hiPSC-derived Schwann cell transplantation as compared to heat killed (Figures 4C–4E). A skilled walking behavioral test was used to quantify locomotion as a readout of nerve and muscle function.[35] Given that Schwann cells derived from all hESC and hiPSC lines comparably improved myelinated axon number and nerve electrophysiology, transplantation was performed with Schwann cells derived from only one hESC and one hiPSC line. H9 (hESC) and GM01582 (hiPSC) were randomly selected for this assay.

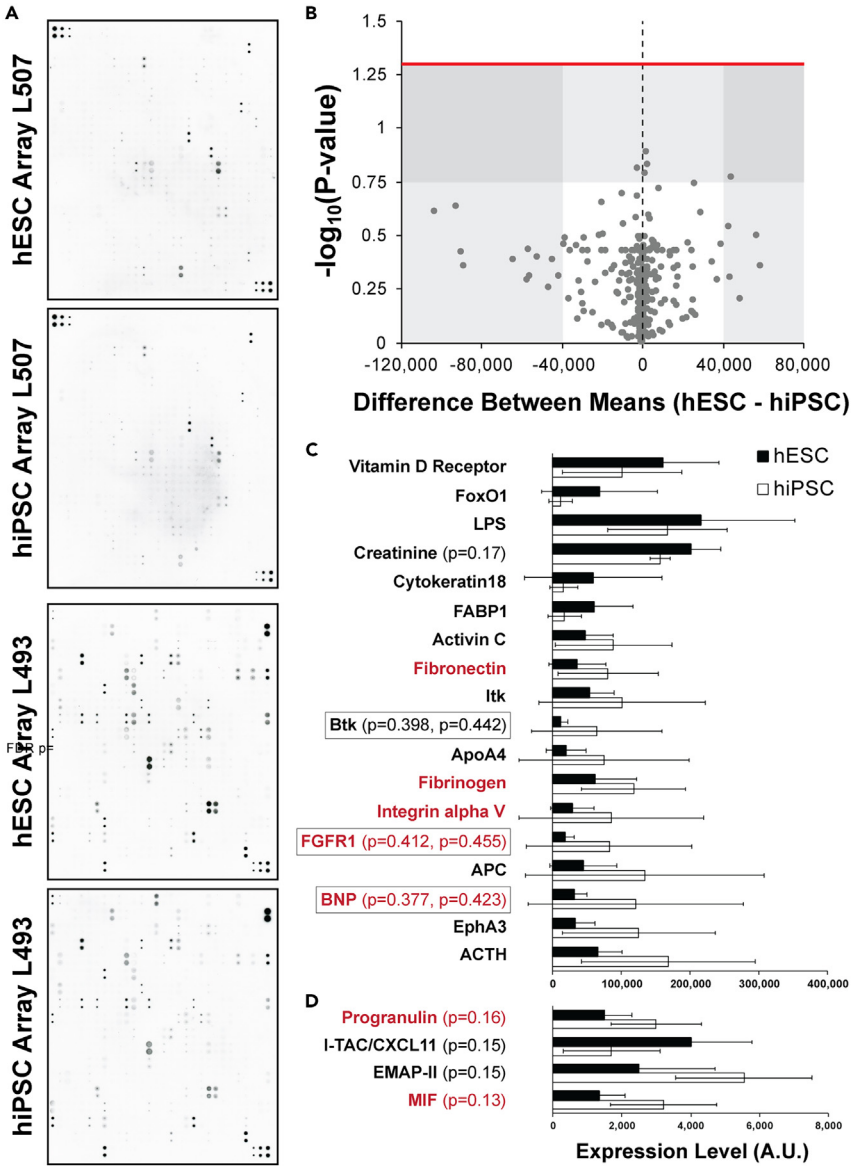

Figure 3. Insignificant proteome differences between hESC- and hiPSC-derived Schwann cells

Protein lysates were collected from passage three hESC- and hiPSC-derived Schwann cells and antibody array was performed. Signal intensity for each protein was averaged and compared between hESC- and hiPSC-derived Schwann cells (n = 1 per stem cell line, n = 3 per stem cell type).

(A) Representative immunoblots are shown.

(B) Differential expression results displayed by volcano plot. Data were analyzed by multiple unpaired t-tests with the false discovery rate approach two-stage step-up method of Benjamini, Kreiger, and Yekutieli method (desired FDR = 1%, significant $p < 0.05$). The red line indicates statistical significance ($p < 0.05$) with no data points reaching significance. The gray boxes highlight proteins that were most divergently expressed (graphed in (C)) and nearest to statistical significance (graphed in (D)). Average expression levels of (C) the most divergently expressed proteins and (D) the proteins nearest to statistical significance. Data are represented as mean ± SD. The p-values for those nearest to statistical significance are shown in parentheses. Proteins in red have concrete links to Schwann cell/myelin function. Equal variance was assessed by F-test analysis and proteins with unequal variance are outlined with a black box. The p-values from both unpaired t-tests (first p-value) and unpaired t-tests with Welch correction (second p-value) are shown for these proteins in parentheses. All data are not significant for both analyses ($p > 0.05$).

After training the mice to walk on a ladder beam, their ability to grasp each rung was subsequently scored as described using an established protocol.[35] The resulting injured hindlimb scores were equivalent between alive hESC- and hiPSC-derived Schwann cells (p = 0.0783, Figure 4F). These findings suggest that hESC- and hiPSC-derived Schwann cells promote axon regeneration and reinnervation of denervated distal foot muscles to a similar extent.

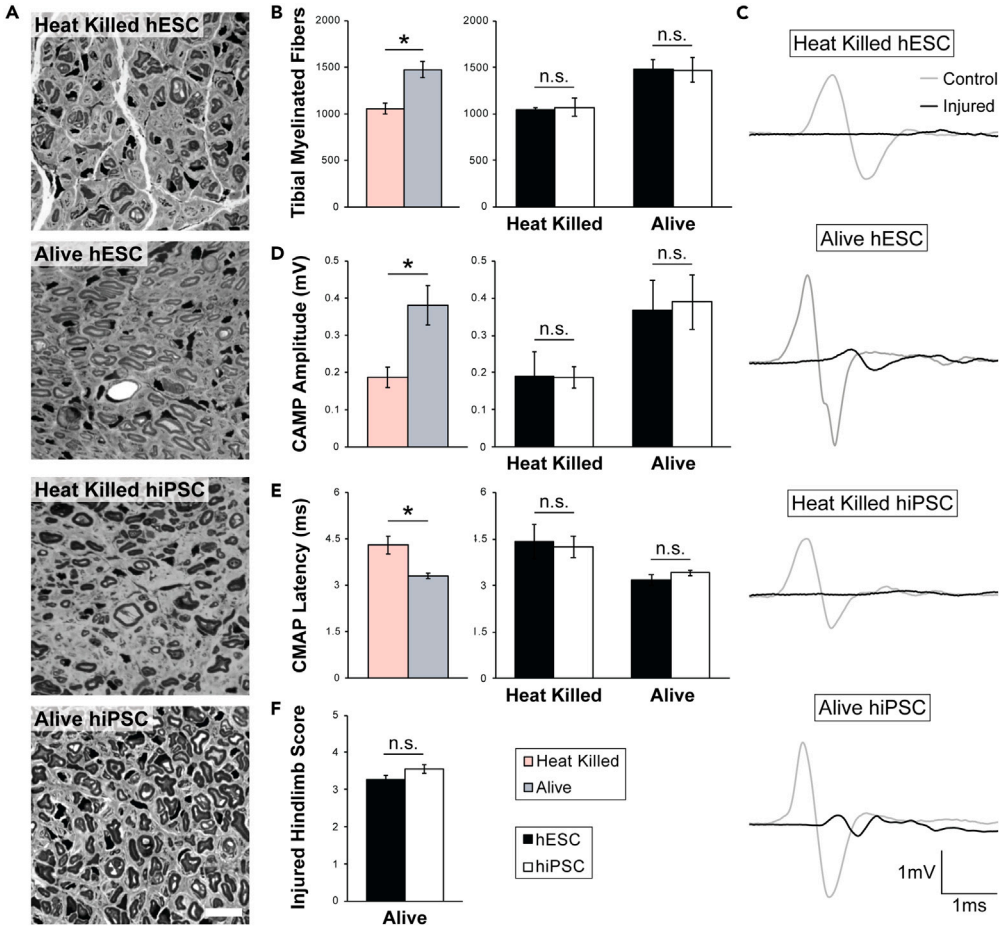

Figure 4. hESC- and hiPSC-derived Schwann cells equally promote regeneration of chronically denervated peripheral nerves

Tibial nerves were chronically denervated, repaired with transected peroneal nerve and heat killed or alive hESC- and hiPSC-derived Schwann cells were injected distal to the lesion. Histological, electrophysiological, and behavioral recovery were evaluated three months post-transplantation.

(A) Representative images of toluidine blue stained tibial nerve cross-sections with transplanted heat killed or alive hESC- and hiPSC-derived Schwann cells. Scale bar, 10μm.

(B) Quantification of tibial nerve myelinated fiber number.

(C) Representative sciatic nerve CMAP traces with transplanted heat killed or alive hESC- and hiPSC-derived Schwann cells. Quantification of CMAP (D) amplitude and (E) latency.

(F) Skilled walking was assessed by ladder beam test with transplanted alive hESC- and hiPSC-derived Schwann cells. Data are represented as mean ± SEM. Heat killed hESC and hiPSC data were pooled (light pink bars) and compared to pooled alive hESC and hiPSC data (light blue bars) to demonstrate improvement with alive cell transplantation. Equal variance was assessed by F-test analysis and the pooled heat killed compared to pooled alive datasets all demonstrated unequal variance (light pink/light blue bar graphs). The hESC- as compared to hiPSC-derived Schwann cells datasets (black/white bar graphs) were analyzed by unpaired t-test due to equal variance and the pooled heat killed compared to pooled alive datasets (light pink/light blue bar graphs) were compared by unpaired t-test with Welch correction. * = significant ($p < 0.05$), n.s. = not significant ($p > 0.05$). Schwann cells derived from all six stem cell lines were evaluated by nerve morphometry and electrophysiology (n for histology/electrophysiology: alive - H1 $n = 2/2$, H7 $n = 3/3$, H9 $n = 3/4$, GM01582 $n = 3/4$, GM02623 $n = 4/4$, GM08398 $n = 4/4$, heat killed - H9 $n = 3/3$, GM01582 $n = 5/5$), whereas only H9 and GM01582 were assessed behaviorally ($n = 4$ each).

DISCUSSION

The field of stem cell differentiation is progressing at a rapid pace. Optimized protocols that improve differentiation efficiency and efficacy are continuously being developed. Schwann cell differentiation protocols are following this trajectory and have gone through several iterations.[36,37] We have developed a Schwann cell differentiation protocol that is efficient and reproducible.[5] The resulting cells exhibit molecular, morphological, and functional characteristics of Schwann cells.[5] Even though the equivalence of hESCs and hiPSCs is controversial, reports comparing cells differentiated from each are scarce. However, in genetically matched hESC and hiPSC lines, transcriptomic variation arising from genetic background overshadows variation due to cellular origin.[38] Here, we sought to determine if hESC- and hiPSC-derived Schwann cells generated with our protocol are molecularly and functionally equivalent in order to justify the sole use of iPSCs for future studies.

hESCs and hiPSCs were similarly differentiated with our protocol and the resulting hESC- and hiPSC-derived Schwann cells were molecularly comparable. Only 0.85% of genes (142 out of 16,590) detected by RNA sequencing were significantly differentially expressed and only a few of these had a concrete (2.82%, 4 out of 142) or potential (9.86%, 14 out of 142) link to Schwann cell/myelin function. *BDNF*, *WNT5A*, *POSTN* and *TXNIP* are the significantly differentially expressed genes at the mRNA level with an established role in Schwann cells. Interestingly, 86% of the significantly differentially expressed genes exhibited increased expression in iPSC-derived Schwann cells and these four genes belong to this group. GO enrichment analysis of genes increased in iPSC-derived Schwann cells as compared to hESC-derived Schwann cells did not reveal major links to nervous system function or provide much insight into the reason for this phenomenon. The molecular similarity of hESC- and hiPSC-derived Schwann cells was also compared by antibody array. None of the 1000 proteins quantified with this assay, including pro-BDNF and BDNF, were significantly differentially expressed. Several additional integral Schwann cell/myelin proteins were also evaluated by the antibody array including ERBB2 ($p = 0.7774$), ERBB3 ($p = 0.7774$), ERBB4 ($p = 0.7643$), GDNF ($p = 0.9595$), NGF ($p = 0.7644$), NGFR ($p = 0.3739$), S100A4 ($p = 0.6219$), S100A6 ($p = 0.4245$) and S100A10 ($p = 0.3658$). We cannot make conclusions about why some genes are elevated at the mRNA level but not the protein level, but this is likely due to complex post-transcriptional regulation that is involved in controlling the expression of these critically important genes. Our results indicate that hESC- and hiPSC-derived Schwann cells generated with our differentiation protocol are molecularly comparable but identify genes that should be taken into consideration for future experimentation and may contribute to line-to-line variability.

In support of our molecular analysis, we also demonstrated that transplanted hESC- and hiPSC-derived Schwann cells function comparably to promote regeneration and reinnervation in a chronic denervation and regeneration mouse model. It is well appreciated that some of the transplanted cells likely myelinated regenerating axons, but the majority primarily promoted regeneration by providing trophic support.[39,40] Myelinated axon number, CMAP amplitude and latency and skilled walking were all equally improved with transplantation of alive hESC- and hiPSC-derived Schwann cells as compared to heat killed cells. These findings further validate our Schwann cell differentiation protocol and provide evidence supporting the molecular and functional equivalence of Schwann cells derived from hESCs and hiPSCs using this protocol. Given the ethical concerns regarding the use of hESCs and the data we report here, we believe iPSCs are an ideal platform for generating human Schwann cells, but it is best to be mindful of the minor differences that we identified as compared to hESC-derived Schwann cells.

Future studies based on this work include exploring the myelination potential of hESC- and hiPSC-derived Schwann cells to determine if gene expression changes in these cells become more evident with maturation and affect myelin sheath function. Unfortunately, current Schwann cell differentiation protocols, including our own, are either unable to myelinate or very inefficiently myelinate neurons *in vitro*.[5,37,41] It may be worth exploring functional differences in hESC- and hiPSC-derived Schwann cells caused by gene expression changes like cell proliferation, migration and elongation. We would also like to note that differentiation protocols requiring FACS sorting introduce multiple variables into the process of differentiation Schwann cells. Although there are benefits to harvesting pure populations of Schwann cells, it would also be advantageous to differentiate Schwann cells and neurons in a co-culture or organoid system in order to create peripheral nerve-like environments with mature myelin sheaths. As Schwann cell differentiation protocols continue to improve, protocols capable of producing pure cultured Schwann cells resembling primary cultured Schwann cells and co-cultures with neurons ensheathed by mature myelin will likely become common practice.

Limitations of the study

Limitations of this study include not being able to compare CD49d-positive cells to CD49d-negative cells to support the conversion to Schwann cells and not being able to analyze the subtypes of Schwann cells differentiated from hESCs and hiPSCs. When developing the Schwann cell differentiation protocol,[5] immunostaining prior to FACS sorting revealed that non-Schwann cell cells generated by this differentiation protocol included Tuj1-positive neurons, presumably sensory neurons since they are neural crest derivatives. We presumed the remaining cells were a combination of neural crest cells, melanocytes, other neural crest derivatives and possibly connective tissue like fibroblasts, but we have not thoroughly characterized them due to low survival after FACs sorting. Additionally, it would be interesting to define the subtype composition of hESC- and hiPSC-derived Schwann cells which could be explored in future studies using single-cell RNA sequencing.

Another limitation of this study was only transplanting Schwann cells derived from one hESC and one hiPSC line for the skilled walking assay to evaluate recovery in the chronic denervation and regeneration animal model. However, Schwann cells derived from all three hESC and all three hiPSC lines were used to evaluate recovery of tibial nerve myelinated fiber density, CMAP amplitude and CMAP latency in this model. The stem cell lines used for the skilled walking assay were randomly selected. Given that hESC- and hiPSC-derived Schwann cells are molecularly comparable and that hESC- and hiPSC-derived Schwann cells equally improved tibial nerve myelinated fiber density, CMAP amplitude and CMAP latency, we elected to use only one hESC and one hiPSC line for functional assessment given that these experiments are labor intensive and to conserve mice.

STAR★METHODS

Detailed methods are provided in the online version of this paper and include the following:

- KEY RESOURCES TABLE
- RESOURCE AVAILABILITY
  - Lead contact

SUPPLEMENTAL INFORMATION

Supplemental information can be found online at https://doi.org/10.1016/j.isci.2024.109855.

ACKNOWLEDGMENTS

This work was supported by Maryland Stem Cell Research Fund Discovery grant (2014-MSCRFI-0715) and Dr. Miriam and Sheldon G. Adelson Medical Research Foundation to Dr. Ahmet Hoke. Dr. Kathryn Moss was supported by a Maryland Stem Cell Research Fund Postdoctoral Fellowship and is currently supported by an NIH K22 Award (K22NS125057) and a Johns Hopkins Merkin Peripheral Neuropathy and Nerve Regeneration Center Grant.

AUTHOR CONTRIBUTIONS

Conceptualization, R.M., G.L. and A.H.; Methodology, B.M.-C., G.L.; Investigation, K.R.M., R.M., R.K., J.T.E., Q.S., P.I.V.; Formal Analysis, K.R.M., R.M., R.K.; Writing – Original Draft, K.R.M., A.H.

Writing – Review & Editing, K.R.M., A.H.; Visualization, K.R.M.; Supervision, G.L. and A.H.; Funding Acquisition, A.H.

DECLARATION OF INTERESTS

The authors have declared no competing interests.

Received: November 7, 2022
Revised: February 11, 2024
Accepted: April 26, 2024
Published: April 30, 2024

REFERENCES

1. Jennings, M.J., Lochmuller, A., Atalaia, A., and Horvath, R. (2020). Targeted Therapies for Hereditary Peripheral Neuropathies: Systematic Review and Steps Towards a 'treatabolome'. J. Neuromuscul. Dis. *8*, 383–400. https://doi.org/10.3233/JND-200546.
2. Bilic, J., and Izpisua Belmonte, J.C. (2012). Concise review: Induced pluripotent stem cells versus embryonic stem cells: close enough or yet too far apart? Stem Cell. *30*, 33–41. https://doi.org/10.1002/stem.700.
3. Puri, M.C., and Nagy, A. (2012). Concise review: Embryonic stem cells versus induced pluripotent stem cells: the game is on. Stem Cell. *30*, 10–14. https://doi.org/10.1002/stem.788.
4. Marei, H.E., Althani, A., Lashen, S., Cenciarelli, C., and Hasan, A. (2017). Genetically unmatched human iPSC and ESC exhibit equivalent gene expression and neuronal differentiation potential. Sci. Rep. *7*, 17504. https://doi.org/10.1038/s41598-017-17882-1.
5. Mukherjee-Clavin, B., Mi, R., Kern, B., Choi, I.Y., Lim, H., Oh, Y., Lannon, B., Kim, K.J., Bell, S., Hur, J.K., et al. (2019). Comparison of three congruent patient-specific cell types for the modelling of a human genetic Schwann-cell disorder. Nat. Biomed. Eng. *3*, 571–582. https://doi.org/10.1038/s41551-019-0381-8.
6. Gu, Y., Wu, Y., Su, W., Xing, L., Shen, Y., He, X., Li, L., Yuan, Y., Tang, X., and Chen, G. (2018). 17beta-Estradiol Enhances Schwann Cell Differentiation via the ERbeta-ERK1/2 Signaling Pathway and Promotes Remyelination in Injured Sciatic Nerves. Front. Pharmacol. *9*, 1026. https://doi.org/10.3389/fphar.2018.01026.
7. Griggs, R.B., Yermakov, L.M., Drouet, D.E., Nguyen, D.V.M., and Susuki, K. (2018). Methylglyoxal Disrupts Paranodal Axoglial Junctions via Calpain Activation. ASN Neuro *10*, 1759091418766175. https://doi.org/10.1177/1759091418766175.
8. Lee, M.M., Badache, A., and DeVries, G.H. (1999). Phosphorylation of CREB in axon-induced Schwann cell proliferation. J. Neurosci. Res. *55*, 702–712. https://doi.org/10.1002/(SICI)1097-4547(19990315)55:6<702::AID-JNR5>3.0.CO;2-N.
9. Chang, H.M., Liu, C.H., Hsu, W.M., Chen, L.Y., Wang, H.P., Wu, T.H., Chen, K.Y., Ho, W.H., and Liao, W.C. (2014). Proliferative effects of melatonin on Schwann cells: implication for nerve regeneration

following peripheral nerve injury. J. Pineal Res. *56*, 322–332. https://doi.org/10.1111/jpi.12125.

10. Pan, B., Jing, L., Cao, M., Hu, Y., Gao, X., Bu, X., Li, Z., Feng, H., and Guo, K. (2021). Melatonin promotes Schwann cell proliferation and migration via the shh signalling pathway after peripheral nerve injury. Eur. J. Neurosci. *53*, 720–731. https://doi.org/10.1111/ejn.14998.
11. Latasa, M.J., Jiménez-Lara, A.M., and Cosgaya, J.M. (2016). Retinoic acid regulates Schwann cell migration via NEDD9 induction by transcriptional and post-translational mechanisms. Biochim. Biophys. Acta *1863*, 1510–1518. https://doi.org/10.1016/j.bbamcr.2016.04.009.
12. Yu, F., Weng, J., Yuan, Y.S., Kou, Y.H., Han, N., Jiang, B.G., and Zhang, P.X. (2018). Wnt5a Affects Schwann Cell Proliferation and Regeneration via Wnt/c-Jun and PTEN Signaling Pathway. Chin. Med. J. *131*, 2623–2625. https://doi.org/10.4103/0366-6999.244116.
13. Bihler, K., Kress, E., Esser, S., Nyamoya, S., Tauber, S.C., Clarner, T., Stope, M.B., Pufe, T., and Brandenburg, L.O. (2017). Formyl Peptide Receptor 1-Mediated Glial Cell Activation in a Mouse Model of Cuprizone-Induced Demyelination. J. Mol. Neurosci. *62*, 232–243. https://doi.org/10.1007/s12031-017-0924-y.
14. Sung, H.Y., Chen, W.Y., Huang, H.T., Wang, C.Y., Chang, S.B., and Tzeng, S.F. (2019). Down-regulation of interleukin-33 expression in oligodendrocyte precursor cells impairs oligodendrocyte lineage progression. J. Neurochem. *150*, 691–708. https://doi.org/10.1111/jnc.14788.
15. Sbai, O., Devi, T.S., Melone, M.A.B., Feron, F., Khrestchatisky, M., Singh, L.P., and Perrone, L. (2010). RAGE-TXNIP axis is required for S100B-promoted Schwann cell migration, fibronectin expression and cytokine secretion. J. Cell Sci. *123*, 4332–4339. https://doi.org/10.1242/jcs.074674.
16. Sonnenberg-Riethmacher, E., Miehe, M., and Riethmacher, D. (2015). Promotion of periostin expression contributes to the migration of Schwann cells. J. Cell Sci. *128*, 3345–3355. https://doi.org/10.1242/jcs.174177.
17. Gisbert Roca, F., André, F.M., Más Estellés, J., Monleón Pradas, M., Mir, L.M., and Martínez-Ramos, C. (2021). BDNF-Gene Transfected Schwann Cell-Assisted Axonal Extension and Sprouting on New PLA-PPy Microfiber Substrates. Macromol. Biosci. *21*, e2000391. https://doi.org/10.1002/mabi.202000391.
18. Yi, S., Yuan, Y., Chen, Q., Wang, X., Gong, L., Liu, J., Gu, X., and Li, S. (2016). Regulation of Schwann cell proliferation and migration by miR-1 targeting brain-derived neurotrophic factor after peripheral nerve injury. Sci. Rep. *6*, 29121. https://doi.org/10.1038/srep29121.
19. Lin, G., Zhang, H., Sun, F., Lu, Z., Reed-Maldonado, A., Lee, Y.C., Wang, G., Banie, L., and Lue, T.F. (2016). Brain-derived neurotrophic factor promotes nerve regeneration by activating the JAK/STAT pathway in Schwann cells. Transl. Androl. Urol. *5*, 167–175. https://doi.org/10.21037/tau.2016.02.03.
20. Thomas, P.D., Ebert, D., Muruganujan, A., Mushayahama, T., Albou, L.P., and Mi, H. (2022). PANTHER: Making genome-scale phylogenetics accessible to all. Protein Sci. *31*, 8–22. https://doi.org/10.1002/pro.4218.
21. Gene Ontology Consortium, Aleksander, S.A., Balhoff, J., Carbon, S., Cherry, J.M., Drabkin, H.J., Ebert, D., Feuermann, M., Gaudet, P., Harris, N.L., et al. (2023). The Gene Ontology knowledgebase in 2023. Genetics *224*, iyad031. https://doi.org/10.1093/genetics/iyad031.
22. Ashburner, M., and Lewis, S. (2002). On ontologies for biologists: the Gene Ontology–untangling the web. Novartis Found. Symp. *247*, 66–80. discussion 80-63, 84-90, 244-252.
23. Edgar, R., Domrachev, M., and Lash, A.E. (2002). Gene Expression Omnibus: NCBI gene expression and hybridization array data repository. Nucleic Acids Res. *30*, 207–210. https://doi.org/10.1093/nar/30.1.207.
24. Xu, J., Zhang, B., Cai, J., Peng, Q., Hu, J., Askar, P., Shangguan, J., Su, W., Zhu, C., Sun, H., et al. (2023). The transcription factor Stat-1 is essential for Schwann cell differentiation, myelination and myelin sheath regeneration. Mol. Med. *29*, 79. https://doi.org/10.1186/s10020-023-00667-w.
25. Brosius Lutz, A., Lucas, T.A., Carson, G.A., Caneda, C., Zhou, L., Barres, B.A., Buckwalter, M.S., and Sloan, S.A. (2022). An RNA-sequencing transcriptome of the rodent Schwann cell response to peripheral nerve injury. J. Neuroinflammation *19*, 105. https://doi.org/10.1186/s12974-022-02462-6.
26. Catignas, K.K., Frick, L.R., Pellegatta, M., Hurley, E., Kolb, Z., Addabbo, K., McCarty, J.H., Hynes, R.O., van der Flier, A., Poitelon, Y., et al. (2021). alphaV integrins in Schwann cells promote attachment to axons, but are dispensable in vivo. Glia *69*, 91–108. https://doi.org/10.1002/glia.23886.
27. Akassoglou, K., Yu, W.M., Akpinar, P., and Strickland, S. (2002). Fibrin inhibits peripheral nerve remyelination by regulating Schwann cell differentiation. Neuron *33*, 861–875. https://doi.org/10.1016/s0896-6273(02)00617-7.
28. Torres-Mejia, E., Trumbach, D., Kleeberger, C., Dornseifer, U., Orschmann, T., Backer, T., Brenke, J.K., Hadian, K., Wurst, W., Lopez-Schier, H., and Desbordes, S.C. (2020). Sox2 controls Schwann cell self-organization through fibronectin fibrillogenesis. Sci. Rep. *10*, 1984. https://doi.org/10.1038/s41598-019-56877-y.
29. Chen, B., Hu, R., Min, Q., Li, Y., Parkinson, D.B., and Dun, X.P. (2020). FGF5 Regulates Schwann Cell Migration and Adhesion. Front. Cell. Neurosci. *14*, 237. https://doi.org/10.3389/fncel.2020.00237.
30. Gu, Y., Xue, C., Zhu, J., Sun, H., Ding, F., Cao, Z., and Gu, X. (2014). Basic fibroblast growth factor (bFGF) facilitates differentiation of adult dorsal root ganglia-derived neural stem cells toward Schwann cells by binding to FGFR-1 through MAPK/ERK activation. J. Mol. Neurosci. *52*, 538–551. https://doi.org/10.1007/s12031-013-0109-2.
31. Fei, X.W., Pan, C.J., He, Y.L., Fang, Y.J., Zhuang, J.L., and Mei, Y.A. (2011). Brain natriuretic peptide modulates the delayed rectifier outward K(+) current and promotes the proliferation of mouse Schwann cells. J. Cell. Physiol. *226*, 440–449. https://doi.org/10.1002/jcp.22352.
32. Hyung, S., Im, S.K., Lee, B.Y., Shin, J., Park, J.C., Lee, C., Suh, J.K.F., and Hur, E.M. (2019). Dedifferentiated Schwann cells secrete progranulin that enhances the survival and axon growth of motor neurons. Glia *67*, 360–375. https://doi.org/10.1002/glia.23547.
33. Nishio, Y., Nishihira, J., Ishibashi, T., Kato, H., and Minami, A. (2002). Role of macrophage migration inhibitory factor (MIF) in peripheral nerve regeneration: anti-MIF antibody induces delay of nerve regeneration and the apoptosis of Schwann cells. Mol. Med. *8*, 509–520.
34. Fu, S.Y., and Gordon, T. (1995). Contributing factors to poor functional recovery after delayed nerve repair: prolonged denervation. J. Neurosci. *15*, 3886–3895. https://doi.org/10.1523/JNEUROSCI.15-05-03886.1995.
35. Cummings, B.J., Engesser-Cesar, C., Cadena, G., and Anderson, A.J. (2007). Adaptation of a ladder beam walking task to assess locomotor recovery in mice following spinal cord injury. Behav. Brain Res. *177*, 232–241. https://doi.org/10.1016/j.bbr.2006.11.042.
36. Hopf, A., Schaefer, D.J., Kalbermatten, D.F., Guzman, R., and Madduri, S. (2020). Schwann Cell-Like Cells: Origin and Usability for Repair and Regeneration of the Peripheral and Central Nervous System. Cells *9*, 1990. https://doi.org/10.3390/cells9091990.
37. Horner, S.J., Couturier, N., Gueiber, D.C., Hafner, M., and Rudolf, R. (2022). Development and In Vitro Differentiation of Schwann Cells. Cells *11*, 3753. https://doi.org/10.3390/cells11233753.
38. Choi, J., Lee, S., Mallard, W., Clement, K., Tagliazucchi, G.M., Lim, H., Choi, I.Y., Ferrari, F., Tsankov, A.M., Pop, R., et al. (2015). A comparison of genetically matched cell lines reveals the equivalence of human iPSCs and ESCs. Nat. Biotechnol. *33*, 1173–1181. https://doi.org/10.1038/nbt.3388.
39. Wang, Y., Zhao, Z., Ren, Z., Zhao, B., Zhang, L., Chen, J., Xu, W., Lu, S., Zhao, Q., and Peng, J. (2012). Recellularized nerve allografts with differentiated mesenchymal stem cells promote peripheral nerve regeneration. Neurosci. Lett. *514*, 96–101. https://doi.org/10.1016/j.neulet.2012.02.066.
40. Yamamoto, T., Osako, Y., Ito, M., Murakami, M., Hayashi, Y., Horibe, H., Iohara, K., Takeuchi, N., Okui, N., Hirata, H., et al. (2016). Trophic Effects of Dental Pulp Stem Cells on Schwann Cells in Peripheral Nerve Regeneration. Cell Transplant. *25*, 183–193. https://doi.org/10.3727/096368915X688074.
41. Van Lent, J., Vendredy, L., Adriaenssens, E., Da Silva Authier, T., Asselbergh, B., Kaji, M., Weckhuysen, S., Van Den Bosch, L., Baets, J., and Timmerman, V. (2023). Downregulation of PMP22 ameliorates myelin defects in iPSC-derived human organoid cultures of CMT1A. Brain *146*, 2885–2896. https://doi.org/10.1093/brain/awac475.
42. Putri, G.H., Anders, S., Pyl, P.T., Pimanda, J.E., and Zanini, F. (2022). Analysing high-throughput sequencing data in Python with HTSeq 2.0. Bioinformatics *38*, 2943–2945. https://doi.org/10.1093/bioinformatics/btac166.
43. Dobin, A., Davis, C.A., Schlesinger, F., Drenkow, J., Zaleski, C., Jha, S., Batut, P., Chaisson, M., and Gingeras, T.R. (2013). STAR: ultrafast universal RNA-seq aligner. Bioinformatics *29*, 15–21. https://doi.org/10.1093/bioinformatics/bts635.
44. Robinson, M.D., McCarthy, D.J., and Smyth, G.K. (2010). edgeR: a Bioconductor package for differential expression analysis of digital gene expression data. Bioinformatics *26*,

139–140. https://doi.org/10.1093/bioinformatics/btp616.

45. Karolchik, D., Hinrichs, A.S., Furey, T.S., Roskin, K.M., Sugnet, C.W., Haussler, D., and Kent, W.J. (2004). The UCSC Table Browser data retrieval tool. Nucleic Acids Res. *32*, D493–D496. https://doi.org/10.1093/nar/gkh103.
46. Schneider, C.A., Rasband, W.S., and Eliceiri, K.W. (2012). NIH Image to ImageJ: 25 years of image analysis. Nat. Methods *9*, 671–675. https://doi.org/10.1038/nmeth.2089.
47. Heine, W., Conant, K., Griffin, J.W., and Höke, A. (2004). Transplanted neural stem cells promote axonal regeneration through chronically denervated peripheral nerves. Exp. Neurol. *189*, 231–240. https://doi.org/10.1016/j.expneurol.2004.06.014.
48. Scheib, J.L., and Höke, A. (2016). An attenuated immune response by Schwann cells and macrophages inhibits nerve regeneration in aged rats. Neurobiol. Aging *45*, 1–9. https://doi.org/10.1016/j.neurobiolaging.2016.05.004.
49. Moss, K.R., Johnson, A.E., Bopp, T.S., Yu, A.T., Perry, K., Chung, T., and Höke, A. (2022). SARM1 knockout does not rescue neuromuscular phenotypes in a Charcot-Marie-Tooth disease Type 1A mouse model. J. Peripher. Nerv. Syst. *27*, 58–66. https://doi.org/10.1111/jns.12483.

STAR★METHODS

KEY RESOURCES TABLE

REAGENT or RESOURCE	SOURCE	IDENTIFIER
Antibodies		
Human Integrin alpha 4/CD49d PE-conjugated Antibody	R&D Systems	Cat# FAB1354P, RRID:AB_2296441
Normal Goat Serum	Jackson ImmunoResearch Laboratories, Inc.	Cat# 005-000-121, RRID:AB_2336990
Anti-S100B antibody produced in rabbit	Sigma-Aldrich	Cat# HPA015768, RRID:AB_1856538
Goat anti-Rabbit IgG (H+L) Highly Cross-Adsorbed Secondary Antibody, Alexa Fluor™ 568	Thermo Fisher Scientific	Cat# A11036, RRID: AB_10563566
Chemicals, peptides, and recombinant proteins		
0.1% Gelatin in Water	StemCell Technologies	Cat# 07903
DMEM, high glucose	Thermo Fisher Scientific	Cat# 11965092
Fetal Bovine Serum, qualified, United States	Thermo Fisher Scientific	Cat# 26140095
DMEM/F-12, HEPES	Thermo Fisher Scientific	Cat# 11330032
KnockOut™ Serum Replacement	Thermo Fisher Scientific	Cat# 10828028
MEM Non-Essential Amino Acids Solution (100X)	Thermo Fisher Scientific	Cat# 11140050
L-Glutamine (200 mM)	Thermo Fisher Scientific	Cat# 25030081
2-Mercaptoethanol	Thermo Fisher Scientific	Cat# 21985023
Human FGF-basic (FGF-2/bFGF) (aa 1-155) Recombinant Protein	Thermo Fisher Scientific	Cat# PHG0264
DPBS, no calcium, no magnesium	Thermo Fisher Scientific	Cat# 14190144
Dispase (5 U/mL)	StemCell Technologies	Cat# 07913
Matrigel® hESC-Qualified Matrix, LDEV-free	Corning Life Sciences	Cat# 354277
Accutase®	Innovative Cell Technologies, Inc.	Cat# AT104
Y-27632	Cell Signaling Technology	Cat# 13624
KnockOut™ DMEM	Thermo Fisher Scientific	Cat# 10829018
Neurobasal™ Medium	Thermo Fisher Scientific	Cat# 21103049
B-27™ Supplement (50X), serum free	Thermo Fisher Scientific	Cat# 17504044
N-2 Supplement (100X)	Thermo Fisher Scientific	Cat# 17502048
SB-431542	Tocris Bioscience	Cat# 1614
LDN-193189	Tocris Bioscience	Cat# 6053
CHIR 99021	Tocris Bioscience	Cat# 4423
DAPT	Tocris Bioscience	Cat# 2634
dibutyrl cyclic AMP	Sigma-Aldrich	Cat# D0627
L-ascorbic acid	BioGems International, Inc.	Cat# 5088177
Poly-D-lysine hydrobromide	Sigma-Aldrich	Cat# P7280
PBS, pH 7.4	Thermo Fisher Scientific	10010023
ReLeSR™	StemCell Technologies	Cat# 100-0483
Deoxyribonuclease I from bovine pancreas	Sigma-Aldrich	Cat# DN25
Schwann Cell Medium	ScienCell Research Laboratories	Cat# 1701
Trypsin-EDTA (0.05%), phenol red	Thermo Fisher Scientific	Cat# 25300054
Paraformaldehyde 32% Aqueous Solution EM Grade	Electron Microscopy Sciences	Cat# 15714
Triton™ X-100	Sigma-Aldrich	Cat# T9284
Alexa Fluor™ 488 Phalloidin	Thermo Fisher Scientific	Cat# A12379

(*Continued on next page*)

Continued

REAGENT or RESOURCE	SOURCE	IDENTIFIER
ProLong™ Gold Antifade Mountant with DNA Stain DAPI	Thermo Fisher Scientifc	Cat# P36931
TRIzol™ Reagent	Thermo Fisher Scientific	Cat# 15596026
Toluidine Blue 0, Certified, C.N. #DcU-10	Electron Microscopy Sciences	Cat #22050
Critical commercial assays		
RNeasy Mini Kit	Qiagen	Cat# 74104
Human L Series Array 1000 Membrane Kit	RayBiotech	Cat# AAH-BLM-1000-2
Deposited data		
RNAseq Datasets	Gene Expression Omnibus (GEO)	Accession Number: GSE208708
Antibody Array Blots	Mendeley Data	https://doi.org/10.17632/k85ygcx787.2
Experimental models: Cell lines		
H1 Human Embryonic Stem Cells	WiCell Research Institute	Cat# WA01, RRID:CVCL_9771
H7 Human Embryonic Stem Cells	WiCell Research Institute	Cat# WA07, RRID:CVCL_9772
H9 Human Embryonic Stem Cells	WiCell Research Institute	Cat# WA09, RRID:CVCL_9773
GM01582 Fibroblasts	Coriell Institute for Medical Research	Discontinued Product, RRID:CVCL_7323
GM02623 Fibroblasts	Coriell Institute for Medical Research	Cat# GM02623, RRID:CVCL_9W88
GM08398 Fibroblasts	Coriell Institute for Medical Research	Cat# GM08398, RRID:CVCL_A4DH
CF6-Neo Mouse Embryonic Fibroblasts, MitC-treated	Thermo Fisher Scientific	Cat# A34964
Experimental models: Organisms/strains		
Mouse: NOD SCID: NOD.Cg-*Prkdc*^{scid}/J	The Jackson Laboratory	Cat# 001303, RRID:IMSR_JAX:001303
Software and algorithms		
HTSeq (version 2.0): High-throughput sequence analysis in Python[42]	Author: Fabio Zanini, Simon Anders, Givanna Putri and contributors	https://htseq.readthedocs.io/en/latest/
STAR spliced read aligner (version 2.4.0)[43]	Author: Alex Dobin	https://github.com/alexdobin/STAR
Bioconductor package EdgeR (version 2.7)[44]	Author: Mark Robinson, Davis McCarthy and Gordon Smyth	https://www.bioconductor.org/packages//2.7/bioc/html/edgeR.html
UCSC Table Browser[45]	Developed by UCSC and members of the International Human Genome Project	https://genome.ucsc.edu/cgi-bin/hgTables
Graphpad Prism 8 (version 9.1.2)	GraphPad Software, LLC.	https://www.graphpad.com/
Zen2 Blue Edition (version 2.0.0)	Zeiss	https://www.zeiss.com/microscopy/en/products/software/zeiss-zen.html
Imaris x64 (version 9.2.1)	Oxford Instruments, Bitplane	https://imaris.oxinst.com/
Scope4	ADInstruments	https://www.adinstruments.com/support/scope
LabChart8 Reader (version 8.1.18)	ADInstruments	https://www.adinstruments.com/products/labchart-reader
ImageJ (version 2.1.0)[46]	Developed by National Institutes of Health	https://imagej.net/
Other		
Falcon® 40 μm Cell Strainer, Blue, Sterile	Corning Life Sciences	Cat# 352340
10-0 Sterile Micro Sutures	AROSurgical Instruments Corporation	Cat# T05A10N10-13
5 μL, Model 75 RN Syringe	Hamilton Company	Cat# 7634-01
Ultra Disposable Stainless Steel Subdermal Needle Electrodes	Natus Medical Store	Cat# 019-475900

RESOURCE AVAILABILITY

Lead contact

Further information and requests for resources and reagents should be directed to and will be fulfilled by the lead contact, Ahmet Höke (ahoke@jhmi.edu).

Materials availability

This study did not generate new unique reagents. Further information and requests for resources such as reagents listed in key resources table should be directed to the lead contact.

Data and code availability

- Both RNA-seq datasets have been deposited at GEO and are publicly available as of the date of publication. Accession numbers are listed in the key resources table. Original antibody array blots have been deposited at Mendeley and are publicly available as of the date of publication. The DOI is listed in the key resources table. Microscopy and nerve conduction data reported in this paper will be shared by the lead contact upon request.
- This paper does not report original code.
- Any additional information required to reanalyze the data reported in this paper is available from the lead contact upon request.

EXPERIMENTAL MODEL AND STUDY PARTICIPANT DETAILS

Human cells

Stem cell experiments were conducted with approval from the Johns Hopkins Institutional Stem Cell Research Oversight Committee. The three human embryonic stem cell lines used in this study (H1 [male, ethnicity/race unknown], H7 [female, ethnicity/race unknown] and H9 [female, ethnicity/race unknown]) were purchased from WiCell Research Institute. The three human induced pluripotent stem cells lines used in this study (GM01582 [11-year-old Caucasian female donor], GM02623 [61-year-old Caucasian female donor] and GM08398 [8-year-old Caucasian male donor]) were previously generated by Gabsang Lee from healthy control dermal fibroblasts purchased from Coriell Institute for Medical Research. RRID for each are provided in the key resources table. All stem cell lines were confirmed to have normal chromosome ploidy by karyotype analysis; hESCs results are recorded in the Human Pluripotent Stem Cell Registry and hiPSCs were evaluated after they were generated by Gabsang Lee. No apparent differences were detected due to biological sex, but our sample sizes were likely insufficient to definitively conclude this.

All stem cell lines were cultured on Mitomycin C-treated CF6-Neo mouse embryonic fibroblast feeder cells (MEFs, Thermo Fisher Scientific, A34964). Six-well plates were coated with 0.1% gelatin in water (StemCell Technologies, 07903) and incubated at 37°C for 30 minutes prior to seeding approximately 300,000 MEFs per well in MEF medium (DMEM [Thermo Fisher Scientific, 11965092] supplemented with 10% FBS [Thermo Fisher Scientific, 26140095]). MEFs were cultured in 5% CO_2 at 37°C overnight before seeding stem cells. Thawed or passaged stem cells were seeded at approximately 20% confluency per well on MEF feeder plates in stem cell medium (400ml DMEM/F-12 [Thermo Fisher Scientific, 11330032], 100ml knockout serum replacement [Thermo Fisher Scientific, 10828028], 5ml 100x MEM non-essential amino acids solution [Thermo Fisher Scientific, 11140050], 2.5ml 200mM L-glutamine [Thermo Fisher Scientific, 25030081], 500µl 2-mercaptoethanol [Thermo Fisher Scientific, 21985023] and 6ng/ml human basic fibroblast growth factor [bFGF, Thermo Fisher Scientific, PHG0264, prepared in DPBS, no Calcium, no Magnesium {Thermo Fisher Scientific, 14190144}]). Undifferentiated stem cells and differentiating/differentiated Schwann cells were cultured in 5% CO_2 at 37°C in an incubator used solely for human stem cells which was routinely screened for mycoplasma contamination. Medium was changed daily, and cells were passaged 1:3 using 5U/ml dispase solution (StemCell Technologies, 07913) approximately every seven days after removing spontaneously differentiated cells/colonies with a P200 pipet tip.

Mouse strains

Animal experiments were conducted with approval from the Johns Hopkins Animal Care and Use Committee. Adult male NOD SCID mice (aged three-months) were obtained from the Jackson Laboratory. RRID provided in the key resources table. Male mice were exclusively used given that no apparent biological sex differences were observed in hESC- and hiPSC-derived Schwann cells and to minimize variability due to the estrous cycle. NOD SCID mice are homozygous for the *Prkdc*^{scid} mutation resulting in the absence of functional T cells and B cells, lymphopenia and hypogammaglobulinemia. They are able to accept allogeneic and xenogeneic grafts making them an ideal model for cell transplantation experiments. Mice used for this study were purchased directly from the Jackson Laboratory, so their backcrossing status, weight and husbandry conditions were monitored and standardized though the Jackson Laboratory. Littermate males were shipped and housed together in individually ventilated cages (Allentown Caging Equipment, PC75JHT) with corn cob bedding (Teklad, 7097). Mice were provided a single cotton nestlet (Ancare Nestlets, NES3600) for enrichment, fed autoclaved global 18% protein extruded rodent diet (Teklad, 2018SX) and provided reverse-osmosis-treated water via an Edstrom automated in-cage watering system (Avidity Science LLC). Cages were changed every two weeks and colony mice were monitored quarterly for pathogens. Mice were randomly assigned to groups for Schwann cell transplantation experiments and differences due to biological sex were not evaluated due to the sole use of male mice.

METHOD DETAILS

Schwann cell differentiation

MEF-conditioned stem cell medium was prepared by adding stem cell medium to MEF feeder plates, collecting the medium after 24 hours and freezing at -20°C. Gelatin coated 10cm dishes (one per three wells of stem cells) were prepared by incubating with 0.1% gelatin in water at 37°C for at least 30 minutes. Matrigel coated 24-well plates were prepared by adding ice-cold LDEV-free, hESC-qualified matrigel (Corning Life Sciences, 354277) to each well (thawed at 4°C overnight) and incubating at room temperature for at least one hour. After removing spontaneously differentiated cells/colonies with a P200 pipet tip, cells were incubated with accutase (Innovative Cell Technologies, Inc., AT104) at 37°C for 20 minutes. Stem cell medium was added to each well, the cells were gently triturated and then passed through a 40μm cell strainer (Corning Life Sciences, 352340). The cells were topped up to 15ml with stem cell medium and centrifuged at 200xg for five minutes at 20°C. Supernatant was removed, and cells were resuspended in MEF-conditioned stem cell medium supplemented with 6ng/ul bFGF and 10μM Y-27632 (Cell Signaling Technology, 13624). Cells were seeded onto matrigel coated 24-well plates, 60,000 cells per well, and medium was changed every two days until reaching 80% confluency which generally takes one to three days.

The stem cells were then differentiated into Schwann cells following a protocol developed by the Lee lab.[5] This involved treatment with small molecules in KSR medium (415ml knockout DMEM [Thermo Fisher Scientific, 10829018], 75ml knockout serum replacement, 5ml 100x MEM non-essential amino acids solution, 2.5ml 200mM L-glutamine and 500μl 2-mercaptoethanol) and/or NB medium (480ml neurobasal medium [Thermo Fisher Scientific, 21103049], 10ml B27 Supplement [Thermo Fisher Scientific, 17504044], 5ml N2 Supplement [Thermo Fisher Scientific, 17502048] and 2.5ml 200mM L-glutamine). On differentiation days zero and one (cells at 80% confluency), all of the stem cell medium was gently removed by aspiration and 500ul of KSR medium supplemented with 10μM SB-431542 (Tocris Bioscience, 1614) and 500nM LDN-193189 (Tocris Bioscience, 6053) was added to each well. Most of the medium was removed to prevent drying on all subsequent medium changes (400μl removed per well, adding 500μl fresh medium each time). One differentiation days two and three, the medium was changed to KSR medium supplemented with 10μM SB-431542, 500nM LDN-193189, 3μM CHIR 99021 (Tocris Bioscience, 4423) and 10μM DAPT (Tocris Bioscience, 2634). On differentiation days four and five, the medium was changed to KSR/NB (3:1) medium supplemented with 3μM CHIR 99021 and 10μM DAPT. On differentiation days six and seven, the medium was changed to KSR/NB (1:1) medium supplemented with 3μM CHIR 99021 and 10μM DAPT. On differentiation days eight and nine, the medium was changed to KSR/NB (1:3) medium supplemented with 3μM CHIR 99021 and 10μM DAPT. On differentiation days 10 through 20, the medium was changed to NB medium supplemented with 200μM dibutyrl cyclic AMP (Sigma-Aldrich, D0627) and 200μM L-ascorbic acid (BioGems International, Inc., 5088177).

Schwann cell FACS sorting and culture

Matrigel coated 12-well plates were prepared by adding ice-cold matrigel to each well (thawed at 4°C overnight) and incubating at room temperature for at least one hour. Poly-D-lysine (PDL, Sigma-Aldrich, P7280, prepared in water) coated coverslips were prepared by placing autoclaved 12mm diameter #1.5 coverslips into a 24-well plate and dotting 100μl of 100μg/ml PDL onto each coverslip 50μl at a time. The plate was incubated at 37°C for at least 30 minutes and then washed several times with PBS (Thermo Fisher Scientific, 10010023). Schwann cells were purified by Fluorescence Activated Cell Sorting (FACS) sorting on differentiation day 21. The medium was gently aspirated, and the cells were washed once with PBS. After removing the PBS, ReLeSR (StemCell Technologies, 100-0483) was added to each well, incubated at room temperature for one minute and removed by gentle aspiration. The dry plate was incubated at 37°C for three minutes and then accutase was added to each well. The plate was tapped against a hard surface five times and the cells were lifted by pipetting with P1000 pipet. The cells in accutase were transferred to a 15ml tube and additional accutase was added up to 5ml. The tube was incubated in a 37°C water bath for 3 minutes with gently agitation every minute. The cells were triturated in a clean 15ml tube 1ml at a time which generally required 8-10 passes through the pipet tip. The dissociated cells were passed through a 40μm cell strainer and MEF medium was added up to 15ml. The cells were centrifuged at 200xg for 10 minutes at 10°C. Supernatant was removed, and cells were resuspended in 1ml FACS Buffer (40ml DPBS, no calcium, no magnesium, 10ml MEF Medium and 100μl 10mg/ml DNaseI [Sigma-Aldrich, DN25]) supplemented with 10μM Y-27632. 50μl of cells were transferred to a 1.5ml tube to use as unstained control and store on ice. The remaining cells were transferred to a 1.5ml tube, 10μl PE-conjugated anti-CD49d antibody (R&D Systems, FAB1354P) was added and the cells were rotated in the dark at 4°C for 30 minutes. The cells were transferred to a 15ml tube, 10ml FACS Buffer supplemented with 10μM Y-27632 was added and the cells were centrifuged at 200xg for 5 minutes at 10°C. Supernatant was removed, cells were resuspended in 10ml FACS Buffer supplemented with 10μM Y-27632 and the cells were centrifuged at 200xg for 5 minutes at 10°C. Supernatant was removed and the cells were resuspended in FACS Buffer supplemented with 10μM Y-27632 at a concentration of approximately five million cells/ml. The cells were transported on ice and sorted at the Johns Hopkins FACS core facility. Singlet CD49d-positive Schwann cells were collected into a tube containing Schwann cell medium (ScienCell Research Laboratories, 1701, 500ml basal medium, 25ml FBS, 5ml Schwann cell growth supplement and 5ml antibiotic solution) supplemented with 10μM Y-27632. Schwann cells were seeded onto matrigel coated 12-well plates, 70,000 cells per well, and PDL coated coverslips in 24-well plates, 35,000 cells per well, in Schwann cell medium supplemented with 10μM Y-27632 (passage one). Medium was changed every two days with Schwann cell medium without supplement. Schwann cells were passaged after reaching 80% confluency which typically required one week. Schwann cells were passaged 1:3 using 0.05% trypsin-EDTA (Thermo Fisher Scientific, 25300054). Passage two hESC- and iPSC-derived Schwann cells were used for RNA sequencing and immunocytochemistry. Passage three hESC- and iPSC-derived Schwann cells were used for antibody array and transplantation.

Schwann cell immunocytochemistry

Passage two hESC- and iPSC-derived Schwann cells plated on PDL coated coverslips were fixed with 4% paraformaldehyde (Electron Microscopy Sciences, 15714) in PBS for 15 minutes at room temperature after reaching 70-80% confluency. The paraformaldehyde was discarded, and the Schwann cell were washed with PBS three times for 10 minutes each. The Schwann cells were permeabilized with 0.1% Triton X-100 (Sigma-Aldrich, T9284) in PBS for 15 minutes with gentle agitation at room temperature and then washed with PBS three times with gentle agitation for five minutes each. Schwann cells were blocked with 5% Normal Goat Serum (Jackson ImmunoResearch Laboratories, Inc., 005-000-121) in PBS for one hour with gentle agitation at room temperature and incubated with primary antibody (1:200 rabbit anti-S100B [Sigma-Aldrich, HPA015768]) overnight with gentle agitation at 4°C. Schwann cells were washed with PBS three times with gentle agitation for 10 minutes each and then incubated with secondary antibody (1:400 Alexa Fluor 488 Phalloidin [Thermo Fisher Scientific, A12379] and 1:1000 goat anti-rabbit Alexa Fluor 568 [Thermo Fisher Scientific, A11036]) for one hour with gentle agitation at room temperature. Schwann cells were washed with PBS three times with gentle agitation for 10 minutes each and mounted onto slides with ProLong Gold Antifade Mountant with DAPI (Thermo Fisher Scientifc, P36931). Z-stacks were acquired using a Zeiss Axio Imager Z1 with a 20X air objective using Zeiss Blue software and final images were prepared with Imaris (Oxford Instruments).

RNA isolation and RNA sequencing

RNA was isolated from hESC- and iPSC-derived Schwann cells at passage two after reaching 90% confluency with TRIzol (Thermo Fisher Scientific, 15596026) following the manufacturer's protocol and subsequently purified with a RNeasy Mini Kit (Qiagen, 74104). The Johns Hopkins Experimental and Computational Genomics core facility evaluated RNA quality with a bioanalyzer, and libraries were prepared using TruSeq Stranded RNA (100 ng, Illumina). Preparation included 100bp paired end reads and sequencing run was carried out using an Illumina sequencing platform. Quality control (QC) was performed on base qualities and nucleotide composition of sequences, to identify problems in library preparation or sequencing. Sequence quality for the dataset described here was sufficient that no reads were trimmed or filtered before input to the alignment stage. Reads were counted using HT-seq (version 2.0)[42] and aligned to the latest Human reference genome (GRch38) using the STAR spliced read aligner (version 2.4.0).[43] Average input read counts were 66.7M per sample (range 54.8 to 76.30M) and average percentage of uniquely aligned reads was 80.6% (range 72.3% to 88.7%). Low count transcripts were filtered, and count data were normalized using the method of trimmed mean of M-values (TMM). Differentially expressed genes (FDR < 0.1) were then identified utilizing the Bioconductor package EdgeR (version 2.7).[44] In the first set, paired information was incorporated into the model to account for pair-specific batch effects, while in the second set, paired information was omitted from the model. FPKM values were based on the gene model using GRCh38 RefSeq downloaded from UCSC table browser.[45]

Antibody array

Protein levels were quantified in passage three hESC- and iPSC-derived Schwann cells with the Human L Series Array 1000 Membrane Kit (RayBiotech, AAH-BLM-1000-2). following the manufacturer's protocol. Briefly, cell lysates were biotinylated and incubated on membranes containing antibodies for 1000 human proteins. Immunoblot with HRP-conjugated Streptavidin was then performed and the membranes were imaged. Relative protein levels were quantified using the RayBio Analysis Tool and signal intensity of all samples were normalized to the negative control value for GM01582 iPSC-derived Schwann cells. Signal intensity for each protein was averaged and compared between hESC- and hiPSC-derived Schwann cells (n=1 per stem cell line, n=3 per stem cell type) and compared by multiple unpaired t-tests (without and with Welch correction for unequal variance) with the false discovery rate approach two-stage step-up method of Benjamini, Kreiger and Yekutieli method in Prism 9 (desired FDR = 1%, significant $p<0.05$).

Literature search for Schwann cell function

A PubMed literature search was performed to investigate links to Schwann cell/myelin function on the following: (1) 142 differentially expressed genes identified by RNA sequencing, (2) 20 significant canonical pathways identified by Ingenuity Pathway Analysis, (3) 18 most divergently expressed genes identified by antibody array and (4) four genes nearest to statistical significance identified by antibody array. The gene and the term "Schwann cell," "myelin" or "oligodendrocyte" were searched in PubMed. A concrete link to Schwann cell function is defined by a research publication demonstrating a functional role for the gene in Schwann cells whereas a potential link to Schwann cell function is defined by a research publication demonstrating a functional role for the gene in oligodendrocytes or expression in Schwann cells without functional data. Percentages were calculated based on the number of concrete and potential links divided by the total number of genes assessed.

Schwann cell transplantation

Three-month-old male NOD SCID mice were used for the established chronic denervation and regeneration animal model.[34] This involved transecting the tibial nerve just distal to the sciatic trifurcation, ligating both the proximal and distal stumps, and suturing distal stump to nearby muscles with 10-0 Sterile Micro Sutures (AROSurgical Instruments Corporation, T05A10N10-13). The contralateral side was kept as an uninjured control. Passage three hESC- and iPSC-derived Schwann cells were trypsinized (0.05% trypsin-EDTA) and prepared at a concentration of 40,000 cells/μl in PBS. Heat killed cells were also prepared by boiling at 100°C for 10 minutes, cooling on ice and boiling again at 100°C for 10 minutes. Four months post-denervation (seven-month-old mice), the distal tibial nerve was transplanted with 2.5μl alive or heat

killed hESC- or iPSC-derived Schwann cells using a Hamilton syringe (model 75 RN syringe, Hamilton Company, 7634-01) and repaired with freshly transected proximal common peroneal nerve using 10-0 Sterile Micro Sutures. The syringe was washed with PBS between cell transplantations. Three months post-repair (10-month-old mice), regeneration was assessed by electrophysiological, histological and behavioral assays.

Nerve electrophysiology

Motor-evoked responses were evaluated using an established protocol.[47] Briefly, under isoflurane anesthesia (flow rate 2 L/min), compound motor action potential (CMAP) in the distal foot muscles was recorded from the injured and contralateral sciatic notch of each mouse upon stimulation with PowerLab (ADInstruments) and subdermal needle electrodes (Natus Medical Store, 019-475900). Amplitude (peak to peak from the strongest recorded response) and latency (delay from stimulation to response onset) were quantified for each animal using Scope 4 and LabChart Reader (ADInstruments).

Nerve morphometry

Immediately following electrophysiological examination, animals were sacrificed by cervical dislocation and 2mm of tibial nerve was harvested 5mm distal to the suture site. Nerve samples were fixed and processed for light microscopy by preparing 0.5μm sections and staining them with 1% toluidine blue (Electron Microscopy Sciences, 22050).[48] Tiled images of the entire nerve cross section were acquired on a Zeiss Axiophot microscope with a 60x objective. The number and density of myelinated axons (healthy axons surrounded by a myelin sheath) were evaluated from four randomly placed squares of equal area in the tibial branch of the sciatic nerve with ImageJ.[46,49] Nerve electrophysiology and morphometry results were averaged and compared between alive transplanted hESC- and iPSC-derived Schwann cells (n=2-4/stem cell line, n=8-12 total) and between heat killed transplanted hESC- and iPSC-derived Schwann cells (n=5-3 total) by unpaired t-test. Transplanted hESC- and iPSC-derived Schwann cell results were also pooled and compared between alive and heat killed cells by unpaired t-test with Welch correction for unequal variance (significant $p<0.05$, Prism 9).

Skilled walking behavior

Behavioral recovery was evaluated with a ladder beam walking task by training the mice at least three times per week for two subsequent weeks and performing the test and analysis using an established protocol.[35] Results were averaged and compared between transplanted H9 hESC-derived Schwann cells and GM01582 iPSC-derived Schwann cells (n=4 each) by unpaired t-test (significant $p<0.05$, Prism 9).

QUANTIFICATION AND STATISTICAL ANALYSIS

All statistical analyses were performed using Prism 9 which included the following tests: F-test for equal variance, unpaired t-test (without and with Welch correction for unequal variance), multiple unpaired t-tests with the false discovery rate approach two-stage step-up method of Benjamini, Kreiger and Yekutieli method (without and with Welch correction for unequal variance) and one-way ANOVA with Tukey's post-hoc. The statistical test used, exact n, definition of what n represents and the definition of center and dispersion for each analysis is located in the figure legends. Randomization was performed for the mouse transplantation studies by randomly selecting mice for each condition from multiple litters. Sample size estimations were based on previous experience with RNA sequencing and standard group sizes for rodent experiments. No data points from any assay were excluded from this study.